Journal of Science and Technology in Transportation Volume 2 Issue 2, 2021
ISSN: 2710-XXXX DOI: 10.XXXX/jstit.202111_1(1).0002

Optimization and Modeling of Voltage Model Flux Observer of Vector Control System for Traction motor

Liujian Zhang[1], Xun Wang[1, *]

[1] Southwest Jiaotong University, Chengdu, Sichuan, China

[*] Corresponding Email, wangxun0323@126.com

Abstract

Traction motor is the equipment for electric energy and mechanical energy conversion of rail transit vehicles, and its control system is very important. Vector control system is a high-performance asynchronous motor control mode, which has been widely used in the traction drive system of rail transit vehicles. Flux estimation is a very important link in vector control system, and it is necessary to optimize flux observer. In this work, Three optimization schemes were analyzed, which are low-pass filter instead of pure integration link, integrator with saturation feedback link and improved voltage model flux observer with limited compensation. Each scheme could effectively reduce the influence of the initial value of the integral on the rotor flux observation. Compared with the three schemes, the improved voltage model flux observer with limited compensation could be effective in eliminating waveform distortion and reducing DC component.

Keywords

Vector control system; Flux observer; Traction motor

1 Introduction

The traction drive system controls the speed and traction force of rail transit vehicles by controlling the speed and torque of traction motor, so the control system of traction motor is one of the cores of rail transit vehicle control [1-3]. The control system of traction motor of rail transit vehicle mainly adopts vector control system and direct torque control system. In the 1970s, F. Blaschke of Siemens first proposed the vector control theory based on magnetic field orientation. The basic idea is to decouple the stator current into excitation component and torque component through coordinate transformation. These two components are independent of each other. The purpose of controlling magnetic field and torque can be realized by controlling them separately, so that the asynchronous motor control has the same excellent performance [4-6] as the DC motor control. In the mid-1980s, Professor M.

ISSN: 2710-XXXX DOI: 10.XXXX/jstit.202111_1(1).0002

Depenbrock of Germany proposed a direct self-control method. Different from the decoupling method used in vector control [7-9], it directly controls the torque of the motor by rapidly changing the slip speed of the motor magnetic field to the rotor, so as to obtain the high-performance state of the torque.

The torque of asynchronous motor is not only related to air gap flux and rotor current, but also depends on the power factor of rotor current. The complexity of its torque makes the control of asynchronous motor [10-12] more difficult. In Figure 1, $\alpha\beta$ is the static two-phase coordinate system of the stator, and MT is the two-phase coordinate system rotating at the synchronous angular speed ω_s of the motor, which call MT coordinate system. If the M-axis of MT coordinate system coincides with the rotor flux space vector, the stator current i_s of asynchronous motor could be decomposed into excitation current component i_M and torque current component i_T along the M-axis and T-axis, where i_M and i_T are decoupled from each other. If the excitation component i_M of stator current is kept unchanged and the torque component i_T is controlled during the speed regulation of the motor [13-15], good dynamic performance could be obtained.

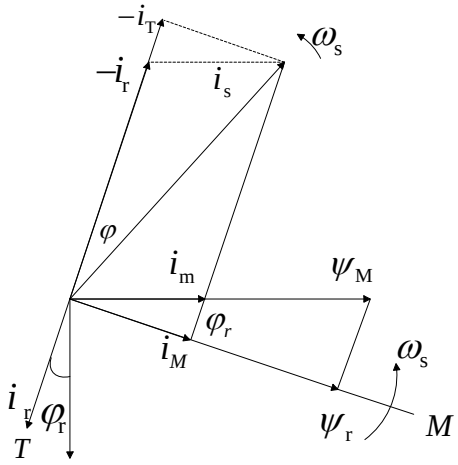

Figure 1 Space vector diagram of traction asynchronous motor.

If the three-phase asynchronous motor can realize MT synchronous coordinate system in the system and ensure that the direction of M-axis is consistent with the direction of rotor magnetic field [16-18]. It can separately control the magnetic field current i_M and torque current i_T to decouple the nonlinear coupling, which is the basic idea of vector control [19-21]. According to the basic concept of vector control, the mathematical model of the control system is established in the synchronous rotating coordinate system based on rotor field orientation. Synchronous rotating coordinate system changes vector control into scalar control. The orientation according to the magnetic field direction makes the system nonlinear decoupling, which is used to improve the dynamic characteristics of the system [22, 23].

In order to obtain the rotor flux accurately, the rotor flux observer is usually used for estimation. At present, there are two commonly used rotor flux observer models: voltage model rotor flux observer and current model flux observer. The current model rotor flux observer could observe the rotor flux in the whole speed range, but because the input signal used contains rotor time constant. The observation

ISSN: 2710-XXXX DOI: 10.XXXX/jstit.202111_1(1).0002

accuracy is related to the measurement accuracy of rotor winding parameters, and the change of temperature and skin effect would lead to a large change range of rotor resistance, it makes it difficult to accurately measure the rotor flux. In this work, the problems of voltage model rotor flux observer could be analysed and optimized.

2 Analysis of problems in voltage model flux observer

In the αβ coordinate system, the rotor flux of the motor could be obtained by integrating the back EMF of the motor. The mathematical expression of the voltage model flux observer is:

$$\begin{cases} \psi_{r\alpha} = \dfrac{L_r}{L_m}\left[\int (U_{s\alpha} - R_s i_{s\alpha})dt - \sigma L_s i_{sa}\right] \\ \psi_{r\beta} = \dfrac{L_r}{L_m}\left[\int (U_{s\beta} - R_s i_{s\beta})dt - \sigma L_s i_{s\beta}\right] \end{cases}$$

The structure diagram of the voltage model rotor flux observer is shown in Figure 2. The voltage model rotor flux observer is essentially a pure integrator. Its algorithm does not contain rotor parameters, so the motor parameters have little effect on it, and there is no speed signal. It is suitable for vector control technology. Its disadvantages are also obvious: first, the DC bias error and initial value error of integration caused by pure integration link. Second, the effect of stator resistance voltage drop at low speed will reduce the observation accuracy. Therefore, the voltage model rotor flux observer is not suitable for low-speed field merging. In order to better control the motor, it needs to be further improved.

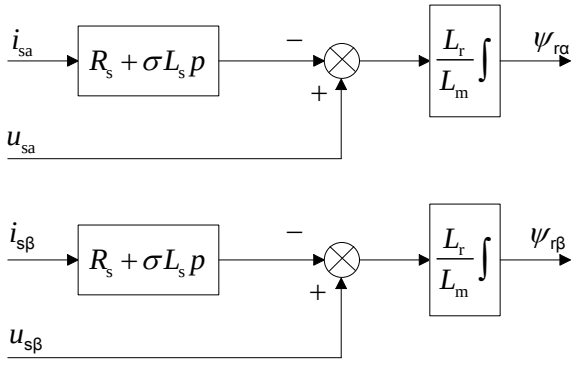

Figure 2 Voltage model of rotor flux linkage in static coordinate system.

Because the voltage model contains pure integration link, and the inherent DC deviation and initial value of integration in the pure integration link would cause the error of flux observation, the inherent initial value of integration and DC deviation of voltage model should be analyzed. If the initial integration time of a sinusoidal signal is not at the peak point of the sinusoidal signal, the output waveform would contain DC component.

ISSN: 2710-XXXX DOI: 10.XXXX/jstit.202111_1(1).0002

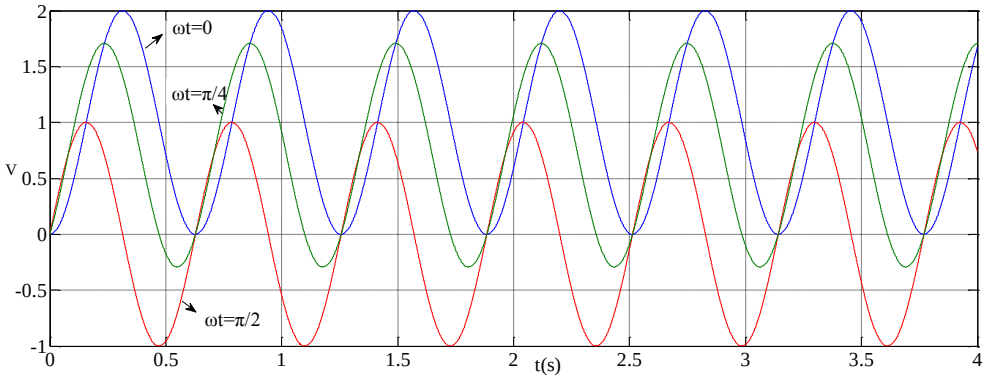

Figure 3 Output waveform with different initial value of integration in pure integral operation of sinusoidal signal.

As can be seen in Figure 3, only when $\omega t = \pi/2$, the waveform is axisymmetric, otherwise the DC component would be large. In addition, the DC offset input would also cause the DC component of the output signal.

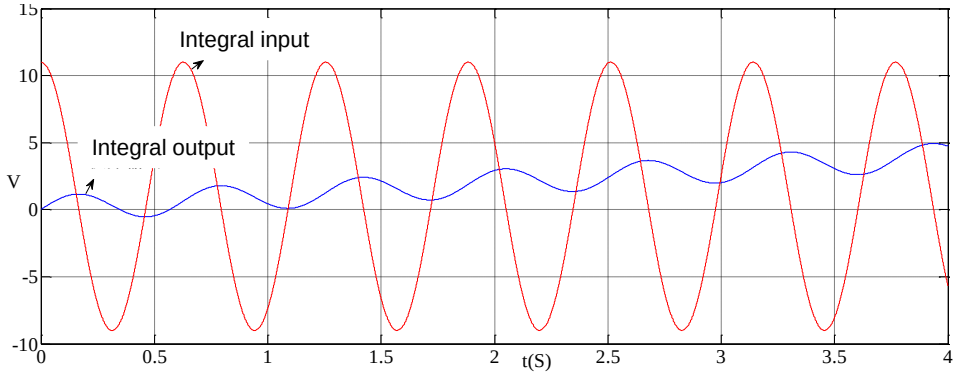

Figure 4 Error caused by DC bias in pure integral operation of sinusoidal signal.

In Figure 4, after the input signal with amplitude of + 10V is injected with DC offset of + 1V, the integral output is divergent. This means that DC bias occurs in the motor, which is prohibited in actual operation, so it should be improved.

3 Improvement of voltage model rotor flux observer

3.1 Low-pass filter instead of pure integral link

Generally speaking, the first-order low-pass filter can be used to replace the pure integral link to eliminate the output error caused by the initial value of the integral, but this method cannot solve the problem of input DC bias, and the introduction of the filter will produce new amplitude and phase angle errors. The principal block diagram of the voltage model rotor flux observer using low-pass filter link instead of pure integration link is shown in Figure 5.

ISSN: 2710-XXXX DOI: 10.XXXX/jstit.202111_1(1).0002

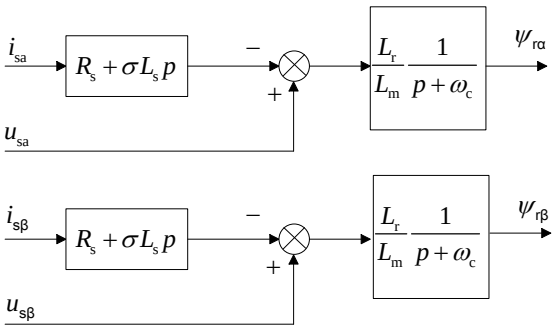

Figure 5 Principal block diagram of the voltage model rotor flux observer using low-pass filter link instead of pure integration link.

Figure 6(a) shows the output waveform of the model at different initial integration values. It can be seen that this method can well reduce the impact of initial integration values on rotor flux observation. As shown in Figure 6(b), waveform 1 is the ideal output waveform, waveform 2 is the output waveform when the cut-off frequency is 20Hz, and waveform 3 is the output waveform when the cut-off frequency is 50Hz. It can be seen that although the low-pass filter can eliminate the influence of the initial integral value, the error of amplitude and phase angle between its output and the ideal output still exists, and the error increases with the increase of the cut-off frequency. Waveform 4 is the output waveform after adding + 1V DC offset to the input signal. It can be seen that the low-pass filter has a certain inhibitory effect on the output divergence caused by DC offset, but its output signal still contains DC component.

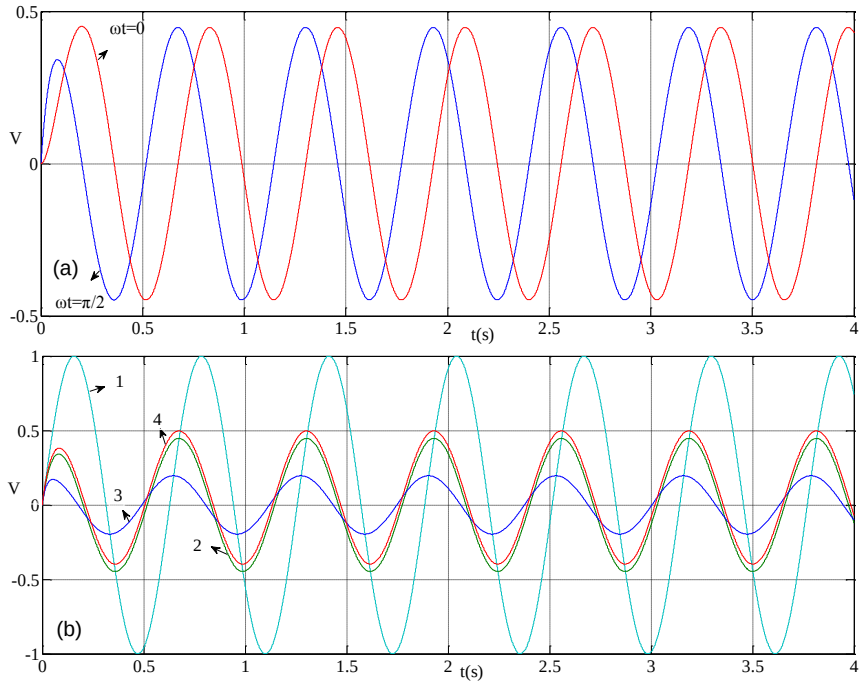

Figure 6 Simulation results of replacing pure integration with low-pass filter.

3.2 Integrator with saturation feedback link

As shown in Figure 7, an integrator with saturation feedback link could compensate the amplitude and phase errors caused by the introduction of low-pass

ISSN: 2710-XXXX DOI: 10.XXXX/jstit.202111_1(1).0002

filter. In the Figure, emf_r is the back electromotive force of the motor, and ψ_{cmp} is the value of ψ_r after amplitude limiting, ω_c is the cut-off frequency and L is the saturation threshold. When ψ_{cmp} =0, the integrator could be regarded as a first-order low-pass filter, when $\psi_{cmp} = \psi_r$, the integrator could be regarded as a pure integrator. The integrator could be regarded as a first-order low-pass filter with adjustable cut-off frequency, and its performance is between pure integrator and low-pass filter.

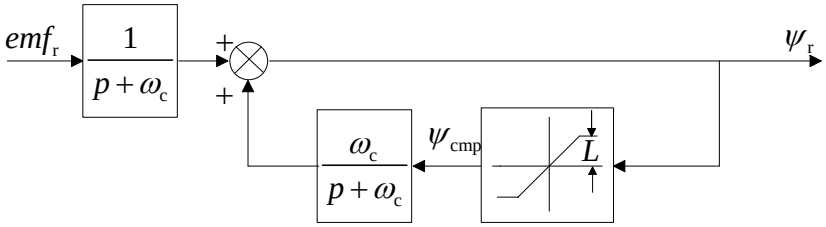

Figure 7 Schematic diagram of integrator with saturation feedback link.

In Figure 8, waveform 1 is the ideal integral output, and waveform 2 is the integral output with saturation feedback link. It can be seen from the figure that the amplitude and phase errors caused by the introduction of low-pass filter have been eliminated. Waveform 3 is the output of the integrator when the DC offset of + 1V is superimposed on the input signal. It can be seen that the DC component is still contained in the output signal, and the waveform is distorted.

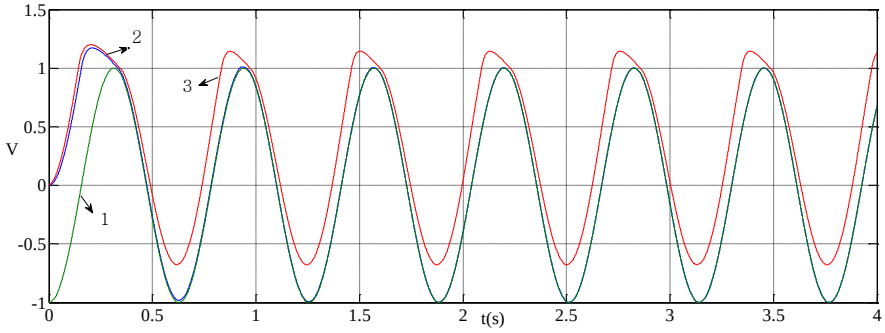

Figure 8 Simulation results of integrator with saturation feedback link.

In this scheme, the selection of saturation threshold L is particularly important. Only when the ideal output amplitude is equal to the saturation threshold could the correct waveform be output, as shown in Figure 9(b). If the saturation threshold is greater than the ideal output amplitude, there is a DC component in the output, as shown in Figure 9(a). The saturation threshold is less than the ideal output amplitude, the output waveform is obviously distorted, and there are certain amplitude and phase errors, as shown in Figure 9(c).

ISSN: 2710-XXXX DOI: 10.XXXX/jstit.202111_1(1).0002

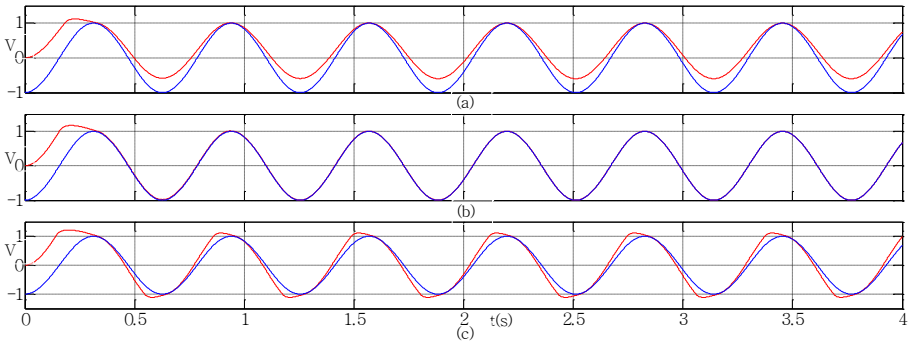

Figure 9 Simulation results of integrator with saturation feedback link when integral amplitude changes.

3.3 Improved voltage model flux observer with finite compensation

Figure 10 is an improved voltage model flux observer with limited compensation. The feedback link of the circuit limits the amplitude of the flux linkage through the transformation and inverse transformation from rectangular coordinates to polar coordinates. The amplitude angle remains unchanged, and the waveform distortion caused by the saturation threshold could be greatly improved.

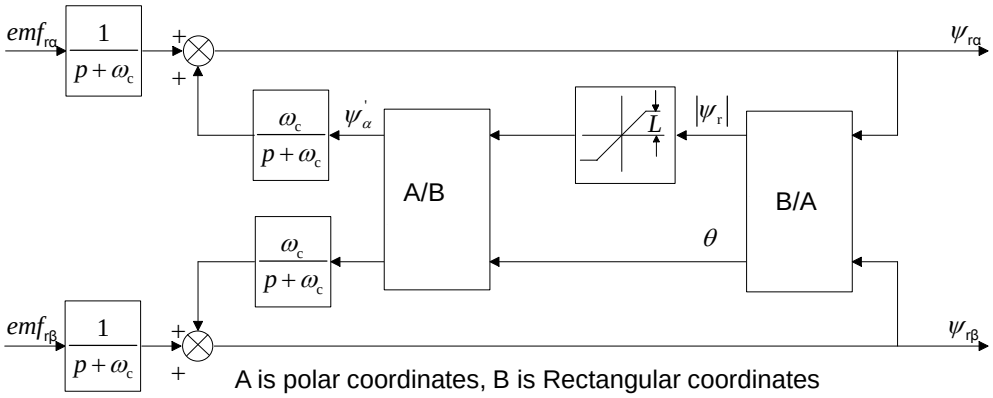

Figure 10 Principal block diagram of improved voltage model flux observer with finite compensation.

Figure 11 shows the simulation results. Waveform 1 is the ideal integral output, and waveform 2 is the output of the improved voltage model with limited compensation. It can be seen from the Figure that the integrator eliminates the amplitude and phase angle errors caused by the introduction of low-pass filter. Waveform 3 is a waveform superimposed with a DC offset of + 1V in the input signal. The DC component in the output signal still exists, but compared with the integrator with saturation feedback link, the DC component is much reduced, and the waveform distortion problem of the integrator with saturation integral feedback link is improved.

ISSN: 2710-XXXX DOI: 10.XXXX/jstit.202111_1(1).0002

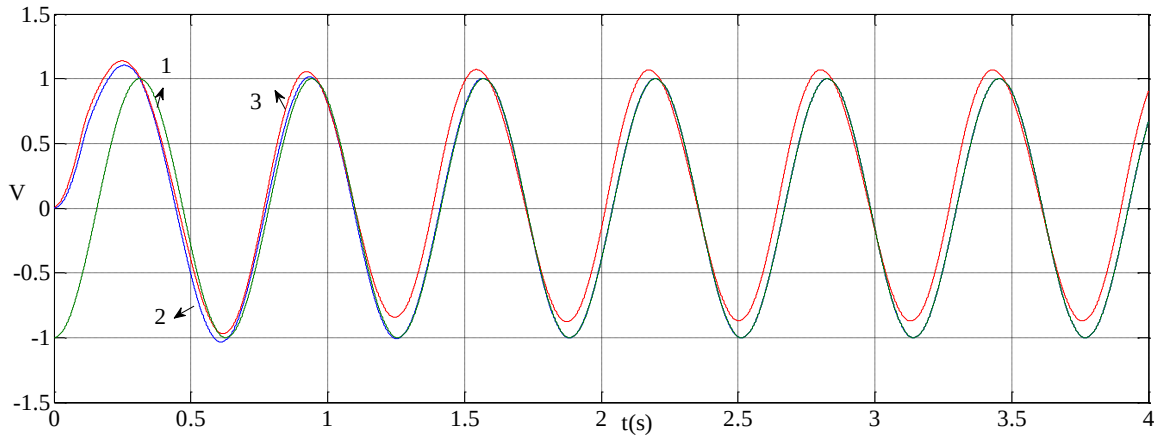

Figure 11 Simulation results of improved voltage model flux observer with finite compensation.

The correct waveform can be output only when the ideal integral output is consistent with the saturation threshold, as shown in Figure 12(b). When the saturation threshold is greater than the ideal integral output value, there is a DC component in the output waveform, as shown in Figure 12(a). When the saturation threshold is less than the ideal integral output value, there are certain phase and amplitude errors in the output waveform, as shown in Figure 12(c). This integrator is suitable for the situation that the magnetic flux amplitude remains unchanged, that is, the ideal output amplitude remains unchanged.

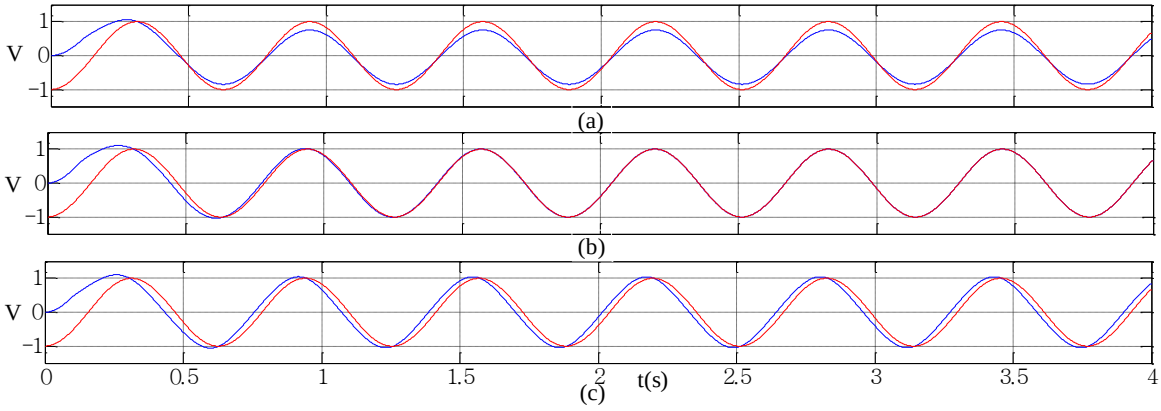

Figure 12 Simulation results of an improved voltage model flux observer with finite compensation when the integral amplitude changes.

Through the analysis and comparison of the above three improved voltage model rotor flux observers, it can be seen that the improved voltage model flux observer with limited compensation has significant effect in eliminating waveform distortion and reducing DC component.

4 Conclusions

Vector control is a high-performance asynchronous motor control method. The stator current is decoupled into excitation component and torque component through coordinate transformation, and the purpose of controlling magnetic field and torque can be realized by controlling them separately. The voltage model rotor flux observer

ISSN: 2710-XXXX DOI: 10.XXXX/jstit.202111_1(1).0002

obtains the rotor flux through estimation. The algorithm does not include rotor parameters, so the motor parameters have little effect on it, and there is no need for speed signal. In the low-pass filter replaces the pure integral link, the simulation results show that the influence of the initial integral value on the rotor flux observation could be reduced. In integrator with saturation feedback link, the simulation results show that the correct waveform could be output only when the ideal output amplitude is equal to the saturation threshold. The improved voltage model flux observer with limited compensation is effective in eliminating waveform distortion and reducing DC component.

Acknowledgements

The authors would like to thank the support from supervisor and acknowledge Southwest Jiaotong University Graduate Scholarship.

References

1. Li M., Wang Y. H., Jia L. M., and Cui Y. R., *Risk propagation analysis of urban rail transit based on network model.* Alexandria Engineering Journal, 2020. **59**(3): 1319-1331.
2. Li S. T., Wu S. R., Xiang S. Q., Zhang Y. B., Guerrero J. M., and Vasquez J. C., *Research on Synchronverter-Based Regenerative Braking Energy Feedback System of Urban Rail Transit.* Energies, 2020. **13**(17).
3. Liu H., Zheng Z. D., and Xu Z., *Architecture of urban rail transit power supply based on PET braking energy feedback.* Journal of Engineering-Joe, 2019(16): 2758-2763.
4. Shen X. J., Wei H. Y., and Wei L., *Study of trackside photovoltaic power integration into the traction power system of suburban elevated urban rail transit line.* Applied Energy, 2020. **260**.
5. Wang L. C., Ping W., Zhao C. Y., Liu D. Y., and Ke W. H., *An experimental study on the characteristics of vibration source in urban rail transit turnouts.* Proceedings of the Institution of Mechanical Engineers Part F-Journal of Rail and Rapid Transit, 2020. **234**(9): 945-957.
6. Yang Y. D., Liu J., Shang P., Xu X. Y., and Chen X. C., *Dynamic Origin-Destination Matrix Estimation Based on Urban Rail Transit AFC Data: Deep Optimization Framework with Forward Passing and Backpropagation Techniques.* Journal of Advanced Transportation, 2020. **2020**.
7. Buchberger H., *The Influence of Thyristor Control on Traction Motors.* IFAC Proceedings Volumes, 1977. **10**(10): 415-419.
8. Denoncin L., Detemmerman B., and Lataire P., *Control of a Current Inverter-Fed Asynchronous Machine for Railway Traction and Alternative Motors in General.* IFAC Proceedings Volumes, 1983. **16**(16): 643-650.
9. Mapelli F. L., Tarsitano D., and Cheli F., *MRAS rotor resistance estimators for EV vector controlled induction motor traction drive: Analysis and experimental results.* Electric Power Systems Research, 2017. **146**: 298-307.
10. Mei T. X., Yu J. H., and Wilson D. A., *A Mechatronic Approach for Anti-slip Control in Railway Traction.* IFAC Proceedings Volumes, 2008. **41**(2): 8275-8280.
11. Pachter M., *Speed control of a field controlled D.C. traction motor.* Automatica, 1981. **17**(4): 627-630.

ISSN: 2710-XXXX **DOI: 10.XXXX/jstit.202111_1(1).0002**

12. Sawma Jean, Seferian Vahe, Khatounian Flavia, Monmasson Eric, and Ghosn Ragi, *An improved anti-rollback control algorithm for gearless traction motor in elevator applications.* Mechatronics, 2021. **79**: 102659.
13. Sen A. K. and Murty A. S. R., *Parallel processing application in traction motor fault diagnosis.* Electric Power Systems Research, 1999. **52**(3): 241-249.
14. Struharňanský Ľuboš, Vittek Ján, Makyš Pavol, and Ilončiak Jaroslav, *Vector Control Techniques for Traction Drive with Induction Machines - Comparison.* Procedia Engineering, 2017. **192**: 851-856.
15. Tian Yang, Zhang Ke, Jiang Bin, and Yan Xing-Gang, *Interval observer and unknown input observer-based sensor fault estimation for high-speed railway traction motor.* Journal of the Franklin Institute, 2020. **357**(2): 1137-1154.
16. Voronin S. G., Kurnosov D. A., Korobatov D. V., and Kulmukhametova A. S., *Effect of Different Winding Switching Methods on Regulating and Energetic Characteristics of Synchronous Motor with Permanent Magnet Excitation.* Procedia Engineering, 2015. **129**: 962-969.
17. Wang Song, Xiao Jian, Huang Jingchun, and Sheng Hanmin, *Locomotive wheel slip detection based on multi-rate state identification of motor load torque.* Journal of the Franklin Institute, 2016. **353**(2): 521-540.
18. Wu Pingbo, Guo Junyu, Wu Hao, and Wei Jing, *Influence of DC-link voltage pulsation of transmission systems on mechanical structure vibration and fatigue in high-speed trains.* Engineering Failure Analysis, 2021. **130**: 105772.
19. Yang Z. G., Xiang D., and Cheng Y. L., *VR Panoramic Technology in Urban Rail Transit Vehicle Engineering Simulation System.* Ieee Access, 2020. **8**: 140673-140681.
20. Zhang W. J., Wu G. P., Rao Z. M., Zheng J., and Luo D. R., *Predictive Power Control of Novel N*3-phase PM Energy Storage Motor for Urban Rail Transit.* Energies, 2020. **13**(7).
21. Zhang Z. S., Wang C. C., Zhou M. L., and You X. J., *Parameters Compensation of Permanent Magnet Synchronous Motor in Flux-Weakening Region for Rail Transit.* Ieee Transactions on Power Electronics, 2020. **35**(11): 12509-12521.
22. Zhang Changfan, Lin Zhenzhen, Liu Jianhua, He Jing, Wu Han, and Li Peng, *Consensus-based total-amount cooperative tracking control for multi-motor locomotive traction system.* Journal of the Franklin Institute, 2019. **356**(2): 819-834.
23. Zou Yingyong, Zhang Yongde, and Mao Hancheng, *Fault diagnosis on the bearing of traction motor in high-speed trains based on deep learning.* Alexandria Engineering Journal, 2021. **60**(1): 1209-1219.